Nexal Membrane Permeability to Anions

PETER R. BRINK and MAYNARD M. DEWEY

From the Department of Anatomical Sciences, Health Sciences Center, State University of New York at Stony Brook, Stony Brook, New York 11794

ABSTRACT The permeability of the septa of the earthworm in the median axon has been calculated for the anions fluorescein and its halogen derivatives. The values ranged from 5.4×10^{-5} to 4×10^{-6} cm/s. Previously, the septa had been shown to contain nexuses. By using freeze-fracture material, the surface area of nexus on the septal membranes was determined to be 4.5%, very similar to the percentage of nexus in the intercalated disk of mammalian myocardium. Plasma membrane permeability to these dyes was also calculated and shown to be much less than that of the septal membranes. In addition, an estimate of cytoplasmic binding for each dye was made, and most dyes showed little or no binding with the exception of aminofluorescein.

Early electron microscope observations of thin sections of many tissues revealed specialized junctional areas of plasma membranes called nexuses which were thought to be low resistance junctions (Dewey and Barr, 1964; Barr et al., 1965; Barr et al., 1968). Similar structures have been described in many other tissues (Robertson, 1963; Martin and Pilar, 1963; Farquahar and Palade, 1963; Pappas and Bennett, 1966).

The work of Barr et al. (1965, 1968) showed that smooth muscle and myocardial cells were electrically continuous. The structure found responsible for current flow from cell to cell was the nexus. Thus, smooth muscle and myocardium can be thought of as being electrical syncytia. In addition, certain neurons and epithelia are also electrically coupled (Furshpan and Potter, 1959; Bennett et al., 1967; Pappas et al., 1971; Loewenstein, 1975).

Evidence has also been compiled to show biochemical cooperation between cells joined by nexuses (Subak-Sharpe et al., 1969; Gilula et al., 1972; Cox et al., 1974; Gilula, 1974). Before cell systems can be called biochemical syncytia, it must be shown that nexal membranes are not absolute barriers to molecular diffusion between cells or that molecules important to the biochemical integration of a tissue can easily diffuse across the nexal membranes. Although the size of molecules that can get through a nexal membrane has been estimated (Weidmann, 1966; Loewenstein, 1975), only a few estimates of nexal membrane permeability to various probes have been made in mammalian myocardium (Weidmann, 1966; Imanaga, 1974; Weingart, 1974; Pollack, 1976).

The purpose of this work was to measure nexal membrane surface area in septal membranes of the giant axon of earthworm and the permeability of the nexus to various fluorescent dyes varying in mol wt from 330 to 835.

The dyes could be excited with a tungsten source. Knowledge of nexal

membrane permeability to the various dyes should allow reasonable estimates of the rate at which biochemical compounds diffuse across a nexus and establish a limit of molecular size that can traverse the nexus.

METHODS

Animals, Saline, and Dissection

Earthworms were purchased from West Jersey Biological (Wenonah, N. J.), and maintained at 4°C in a mixture of mulch and soil. Saline was prepared as described by Prosser and Brown (1950) with a trihydroxymethylamine (Tris) buffer (pH 7.2). Osmolarity of the saline (245 mosmol) was measured by an Advanced Digimatic osmometer (Advanced Instruments, Inc., Needham Heights, Mass.). Nerve cords were dissected as described by Kao and Grundfest (1957) and placed in a chamber as described by Brink and Barr (1974, 1977). Stimulating electrodes were placed at both ends of the nerve cord so that action potentials could be elicited from both directions.

Freeze-Fracture

Nerve cords were fixed in 1.5% glutaraldehyde and 0.1 M Na cacodylate buffer for 4 h followed by a 12-h exposure to 40% glycerol in 0.1 M Na cacodylate buffer. 3-mm lengths of nerve cord, dorsal side up, were rapidly frozen in liquid Freon 22 (Virginia Chemicals Inc., Portsmouth, Va.) and liquid nitrogen and were fractured and replicated at −115°C (pressure, 5×10^{-6} t) on a Balzers BF 300 freeze-etch device (Balzers High Vacuum Corp., Santa Ana, Calif.). Platinum carbon shadowing by an electron gun was employed within 2–3 s of cleavage and was followed by a 20-nm coating of carbon onto the replica. Replicas were cleaned with Clorox (The Clorox Company, Oakland, Calif.), rinsed in distilled water, and picked up on slot grids (Formvar coated, Monsanto Company, St. Louis, Mo.). Axons were easily identified because they are myelinated and large (Bullock and Horridge, 1965). The septa traverse the cytoplasm and are easily distinguished in the midst of large cytoplasmic expanses.

Freeze-fractured septa were photographed, and the total area of septal membrane was calculated using an automated planimeter (Numonics Corp., Landsdale, Pa.). It was assumed the surface was flat. In each micrograph the total number of particles or pits were counted so an estimate of total nexus surface area could be made.

All electron microscope observations were made on an Hitachi 12 electron microscope (Hitachi Ltd., Tokyo, Japan), and all images are printed as positive images.

Dyes and Their Injection

Fluorescein (mol wt 333), dichlorofluorescein (mol wt 401), dibromofluorescein (mol wt 490), diiodofluorescein (mol wt 588), tetrabromofluorescein (mol wt 652), tetraiodofluorescein (mol wt 835), and aminofluorescein (mol wt 342) were purchased from Eastman Kodak Co. (Rochester, N.Y.). Each dye was dissolved in 1.5 M KOH so that its final concentration was 0.3–0.4 M. The solutions were then slowly titrated with H_3PO_4 to pH 7.6–7.8.

Microelectrodes were made on a David Kopf vertical puller (David Kopf Instruments Inc., Tujunga, Calif.). Their resistance ranged from 15 to 50 Mohms regardless of the dye used. The electrodes were connected to a WPI amplifier (model 4M-A, W-P Instruments, Inc., New Haven, Conn.), which in turn had input to a Tektronix D10 oscilloscope (Tektronix, Inc., Beaverton, Oreg.). A Tektronix 160 series was used for pulse generation. Once a dye electrode was inserted into an axon it was used to monitor the resting potential and action potential of the axon. Fluorescein, dichlorofluorescein,

and dibromofluorescein were iontophoresed by applying hyperpolarizing pulses of 20–30 nA, with a 100-ms duration every 120 ms. The iontophoretic period lasted 30 min. Aminofluorescein was iontophoresed by application of a depolarizing pulse with the same amplitude, frequency, and duration as fluorescein. Diiodofluorescein, tetrabromofluorescein, and tetraiodofluorescein were iontophoresed by applying hyperpolarizing pulses of 10–20 nA with 100-ms duration every 120 ms for 60–80 mins.

Permeability Calculation

Fluorescence was monitored by a Zeiss ultraphot microscope (Carl Zeiss, Inc., New York). A tungsten source was used with a BG12 excitor filter for dye excitation. A Zeiss barrier filter (530 nm) was used to observe dye fluorescence. The absorption spectra varied from 489 nm for aminofluorescein to 516 nm for tetrabromofluorescein. The emission spectra varied from 535 to 565 nm (Berlman, 1971).

Within 1–2 min after the termination of the dye injection period, injected cells were photographed with an exposure of 40 s. Preparations were kept in total darkness, except during photographic periods. 40-s exposures were made at varying time intervals.

The concentration of the dye in the injected cells was estimated by microdensitometric and spectrophotometric methods. Both methods gave similar results. First, glass tubes were drawn out so that the inside diameters were 50–100 μm (the outside diameter 250 μm) and were filled with dye concentrations ranging from 0.1–1.0 mM. The filled tubes were photographed under the same conditions as the injected cells. Microdensitometric scans of the negatives allowed a standard against which the density of the negative of the injected cell could be compared and concentration could be estimated (Fig. 1). The greater the dye concentration, the greater the density; therefore, the greater the peak height given by the microdensitometric scan. The peaks were measured in centimeters from the base line and plotted against the concentration of the dye. Scans were made across the negatives perpendicular to the long axis of the dye-filled tubes. Comparison of the peaks of injected cells with those in Fig. 1 allowed an estimate of the dye concentration in the cell. There was a great deal of variation in these measurements but it did allow estimates of cellular dye concentrations.

A second method involved iontophoresis of a dye into a 300-μl cuvette (Precision Cells Inc., Hicksville, N. Y.) containing 0.2 M KCl. The iontophoretic period was the same as that used for dye injection of the axon. A dual beam spectrophotometer (Amicon DW-2UV-VIS, Amicon Corp., Lexington, Mass.) was used to determine the concentration of dye in the cuvette. The absorption peak observed was compared with a standard of absorption vs. dye concentration made from known concentrations (Fig. 2).

The volume of the injected cell was calculated from the cell diameter and length as revealed by the dye injection assuming the cell approximated a cylinder. Because the iontophoretic period for a specific dye was the same for the axon and the cuvette, multiplying the ratio of the cell volume to cuvette volume by the concentration of dye in the cuvette as calculated spectrophotometrically, the concentration of dye in the cell was determined.

Microdensitometric tracings (Joyce, Loebl model III, Joyce, Loebl and Co., Ltd., Gateshead-on-Tyne, England) were made of negatives taken just after termination of the dye injection period (t=1 min). Negatives taken at various time intervals after termination of dye injection were also scanned at varying time intervals. The area under the curves obtained from the microdensitometric scans decreased slightly with increasing time. This loss was thought to be due to dye efflux across the plasma membrane and quenching. The shift in the area from one time to another indicated that dye had diffused across the septa. Areas under the curves were calculated with an automated planimeter (Numonics Corp.). Negatives of dye injections taken with the ultraphot microscope had magnifica-

tions of ×39. The window width was 5 mm and the slit width was 1 mm on the microdensitometer.

The area under the curve was proportional to the dye concentration in that cell. Therefore, by calculating the shift in area under the curve of the injected cell to the

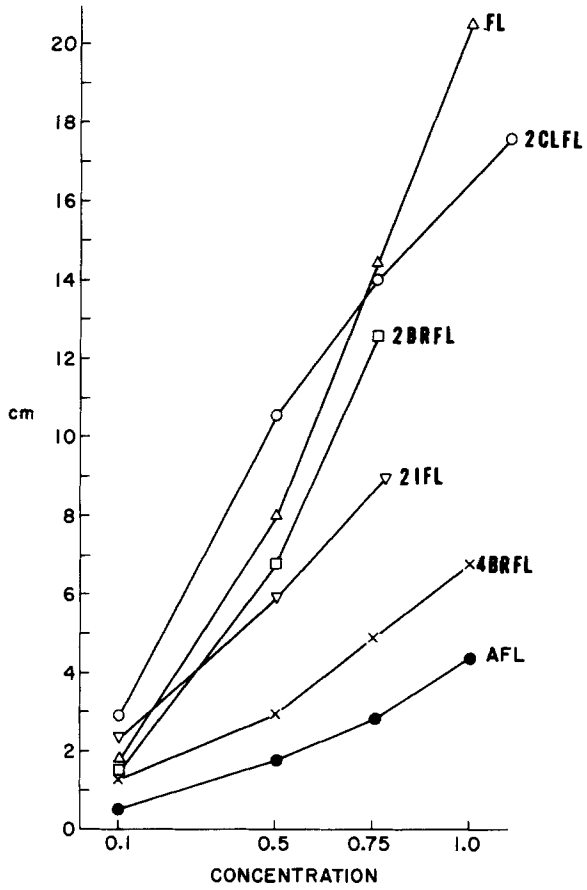

FIGURE 1. Tubes (inside diameter ≤100 μm) filled with various dye concentrations were photographed in the same manner as injected cells. Microdensitometric scans show an approximate proportionality between concentration and peak height. The peak heights were plotted (centimeters) against concentration. Microdensitometric scans were made from the negatives of the tubes. The scans were made perpendicular to the long axis of the tubes. The peak density gave the largest deviation from the base line and was measured in centimeters to give the peak height. FL = fluorescein, 2CLFL = dichlorofluorescein, 2 BRFL = dibromofluorescein, 2 IFL = diiodofluorescein, and 4 BRFL = tetrabromofluorescein. Concentrations of the various dyes ranged from 0.1 to 1.0 mM.

adjacent cells for a specific time interval, the flux of a dye across each septal membrane could be computed. The amount of dye that traversed a septum in a given time interval multiplied by cell volume gave the number of moles that diffused across the septum. The mole number was divided by the surface area of nexus on the septal membrane times the

time interval which gave flux (moles/centimeters^2·second). Nexus surface area was estimated to be 4.5% of the septum from freeze-fracture data given in Table I. The septa traverse the axon at an oblique angle of 140° with little folding of the septal membranes (Stough, 1930; Gunther, 1971, 1975). Therefore, the total septal membrane has been estimated as being approximately 2–2.5 times the cross-sectional area of the axon. 4.5% of that value was taken as the conducting surface of the septum. Dividing the flux by the differences in the dye concentration of the injected and the adjacent cell gives nexal membrane permeability (Katz, 1966). The average dye concentration was used for the computations. Permeability values were calculated at varying time intervals on any one preparation.

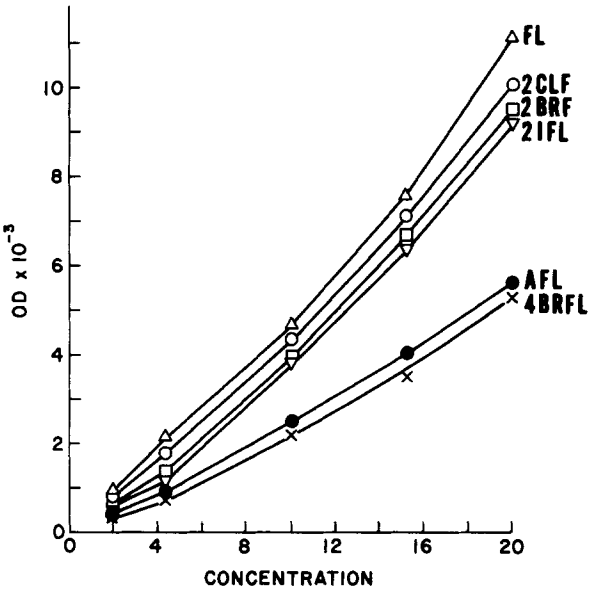

FIGURE 2. Optical density (OD) was plotted against dye concentration. Each dye had a maximum absorption wavelength. Fluorescein (FL) had an absorption peak at 491 nm, dichlorofluorescein (2 CLFL) had a peak at 500 nm, dibromofluorescein (2 BRFL) had a peak at 507 nm, diiodofluorescein (2 IFL) had a peak at 516 nm, and aminofluorescein (AFL) had a peak at 489 nm. The concentration ranged from 4 to 200 nM.

For charged or neutral molecules moving through a membrane where the electrical field is zero, the permeability of that molecule can be calculated by division of the influx of that molecule by external concentration or the efflux of that molecule by the internal concentration (Katz, 1966). Therefore:

$$P_n = M_s/C, \tag{1}$$

where P_n = nexal membrane permeability (the nexal membrane permeability equals the septal membrane permeability); M_s = flux (moles/cm^2·s), the number of moles which traverse the nexal membranes of the septal membrane over a given time interval; and C = the concentration of dye in the injected cell minus the concentration in the adjacent cell.

For the movement of charged molecules in a membrane with an electrical field, the flux of a molecule is dependent on both concentration and the electrical field. If it is assumed that dV_m/dx is constant through the membrane, then the constant field equation (Goldman, 1943; Hodgkin and Katz, 1949) describing the efflux of a molecule through the plasma membrane can be used:

$$M_m = P_m \frac{FV_m}{RT} \frac{(C_m) \exp - (FV_m/RT)}{1 - \exp - (FV_m/RT)} \tag{2}$$

and

$$P_m = \frac{M_m}{\left(\frac{FV_m}{RT}\right)\left(\frac{(C_m) \exp - (FV_m/RT)}{1 - \exp - (FV_m/RT)}\right)}, \tag{3}$$

where F, R, and T have their usual significance, P_m = plasma membrane permeability, M_m = efflux of dye across the plasma membrane, V_m = −80 mV, and C_m = the concentration of dye in the injected cell.

TABLE I
NEXUS SURFACE AREA

Septal membrane area $9.63\times10^3\pm5.6\times10^3$ μm^2 (n=19)	Nexal particles/μm^2 292±210 (n=16)
Average total nexal surface area 4.32×10^2 μm^2	Average total channel area 8.8 μm^2
Cell volume 3.4±1.7 nl (n=19)	
Axon diameter 65±17 μm (n=19)	

Fluorescence Decrease with Light Exposure

Experiments were performed in an attempt to measure the amount of decrease in fluorescence in time with exposure of the dyes to light. Tubes were drawn out to 40-μm diameters with 1-cm lengths. They were filled with 0.5 mM dye and the tube ends sealed. The tubes were photographed with 40-s exposures at varying time intervals. Densitometric scans were made of each exposure, and the area under the curve was calculated.

With such photographic exposure no more than 1% of the total area of densitometric scans was lost with any of the dyes. The interval of time in total darkness between exposures was independent of fluorescence loss. The longer the light exposure, the greater the loss.

Dye Binding

A Bio-Rad dialysis apparatus (Bio-Rad Laboratories, Richmond, Calif.) was used to determine the extent of cytoplasmic binding of each dye. A 5-ml sample of 0.2 M KCl and 40 μM of dye with no cytoplasmic protein was dialyzed against 100 ml of 0.2 M KCl and equilibrium was attained within 3 h for all the dyes. Earthworm nerve cords were homogenized and spun at 40,000 g for 30 min. The 5 ml of supernate containing 1 mg/ml protein (determined by the Lowry method) and a dye concentration of 40 μM was dialyzed against 100 ml of 0.2 M KCl for 3 h. Any difference in the absorption between the sample and the 100-ml vol after computation of the dilution factor (21:1) was taken to be caused by binding. If the average molecular weight of proteins was assumed to be 1×10^4–1.5×10^4 then the ratio of protein to dye was 2:1. Table II gives a summary of

binding for all the dyes. The binding values are estimates, and it should be noted that the homogenates may not behave at all in binding properties like a living neuron.

RESULTS

No alteration in the action potential or resting potential could be observed before or after iontophoresis of any of the seven dyes. When preparations were impaled, if the resting potentials were <-60 mV and action potential height <80 mV, the preparations were discarded.

Morphological studies of the septa were initiated by Stough (1930), and by using light microscopy, he showed that the septa traverses the axon with relatively little folding. Gunther (1975) reconfirmed the simple shape of the septum with no folding using electron microscopy. Investigation of the septa by Hama (1959) showed the membranes to be closely opposed, and vesicles were shown in close association with the septal membranes. Dewey and Barr (1964) showed the septa contained nexuses. Fig. 3 shows electron micrographs of

TABLE II
INTRACELLULAR DYE CONCENTRATIONS AND CYTOPLASMIC BINDING

Dye	Initial dye concentration	Cytoplasmic binding
	mM	%
Fluorescein	0.41±0.2 (n=4)	6
Dichlorofluorescein	0.44±0.28 (n=5)	3
Dibromofluorescein	0.50±0.3 (n=3)	>1
Diiodofluorescein	0.12±0.01 (n=3)	2
Tetrabromofluorescein	0.17±0.08 (n=3)	>1
Aminofluorescein	0.20±0.15 (n=2)	50

freeze-fractured median giant axon septa. Particles ranging in size from 11 to 15 nm in diameter are in the P face (Branton et al., 1975) with pits in the E face.

Fig. 3 shows three different appearances for septal membranes. In Fig. 3*a* there is some folding of the septum but this is seen rarely. The nexal particles are loosely aggregated and are numerous over the surface of the septal membrane. In many cases the septal membranes have only a few nexal particle aggregates (Fig. 3*b*). Anywhere along the septum, vesicles like those seen in Fig. 3*b* may be seen (Hama, 1959). The vesicles are the same size as those seen in thin section (Hama, 1959). A third case is typically seen in the septum (Fig. 3*c*) where the particles and pits are not aggregated but are separated. The spacing varies but is usually about 26 nm. Typically, the particles are found in the P face and pits are in the E face. The septum has an unusual number of particles which appear on the E face (Fig. 3*c*).

Fig. 4 illustrates two densitometric tracings made 1 and 15 min after termination of iontophoresis of the dye, dichlorofluorescein. Photographs of the negatives used to make the microdensitometric tracings are also included in Fig. 4. Note the shift in the curve with time indicating that dichlorofluorescein diffused beyond both septa. All the other dyes used showed similar shifts but the amount of dye that diffused through the septa for a given time interval diminished with increasing molecular weight.

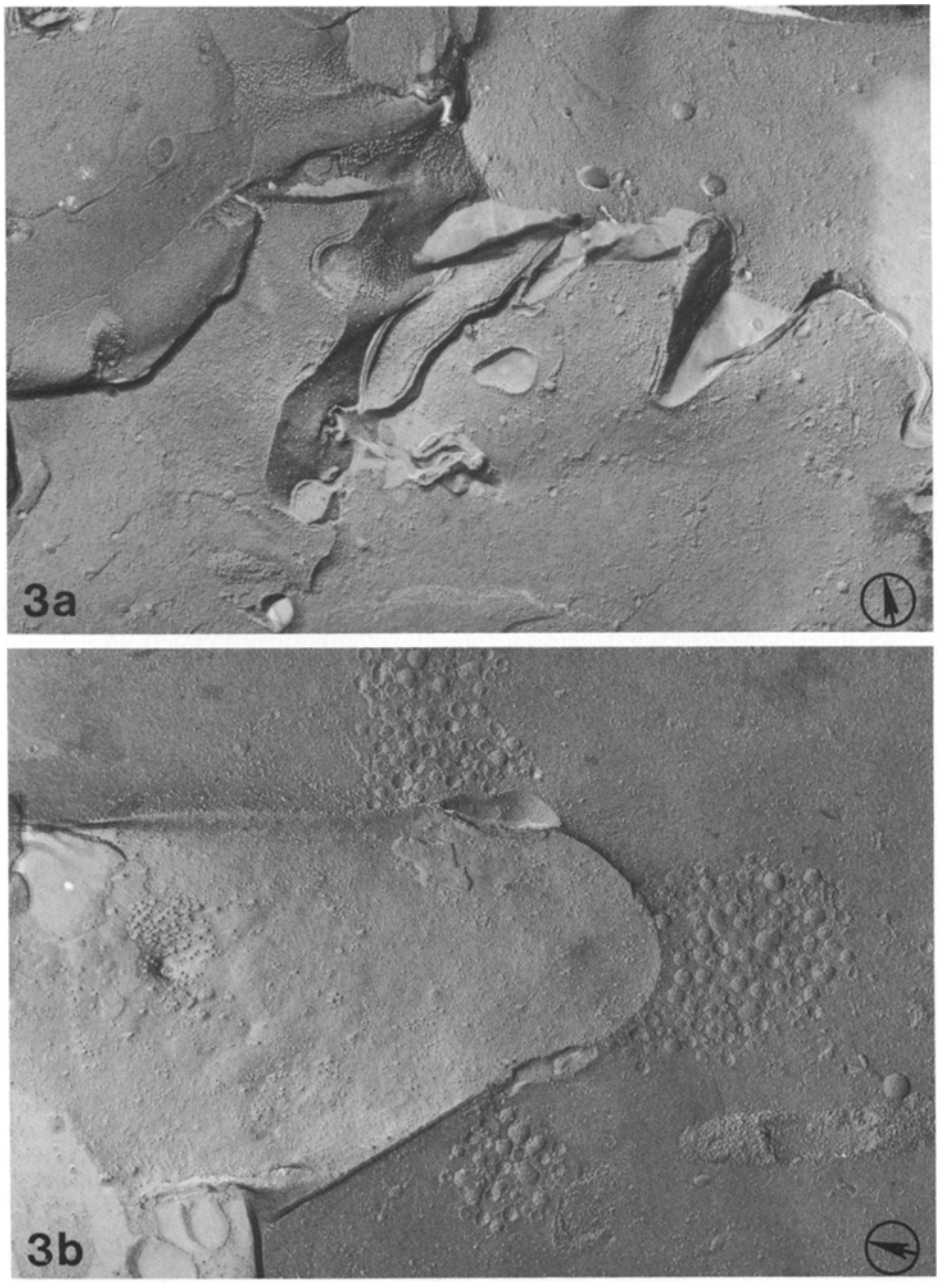

FIGURE 3. (*a*) Freeze-fracture of earthworm median giant axon septum. Particles (connexions) are found predominantly in the P face and are loosely aggregated. Magnification × 29,620. (*b*) Freeze-fracture of septum showing a loosely aggregated nexus but an otherwise junction-free surface. Note also the vesicles in the cytoplasm adjacent to the septum. The vesicles varied in size from 95.0 to 40.0 nm. Magnification × 37,000. (*c*) Freeze-fractured septum where the pits and particles are spaced. The membrane surface is relatively flat. There are a large number of particles which appear in the E face. Magnification × 43,900. Arrows in lower right corner indicate shadow direction.

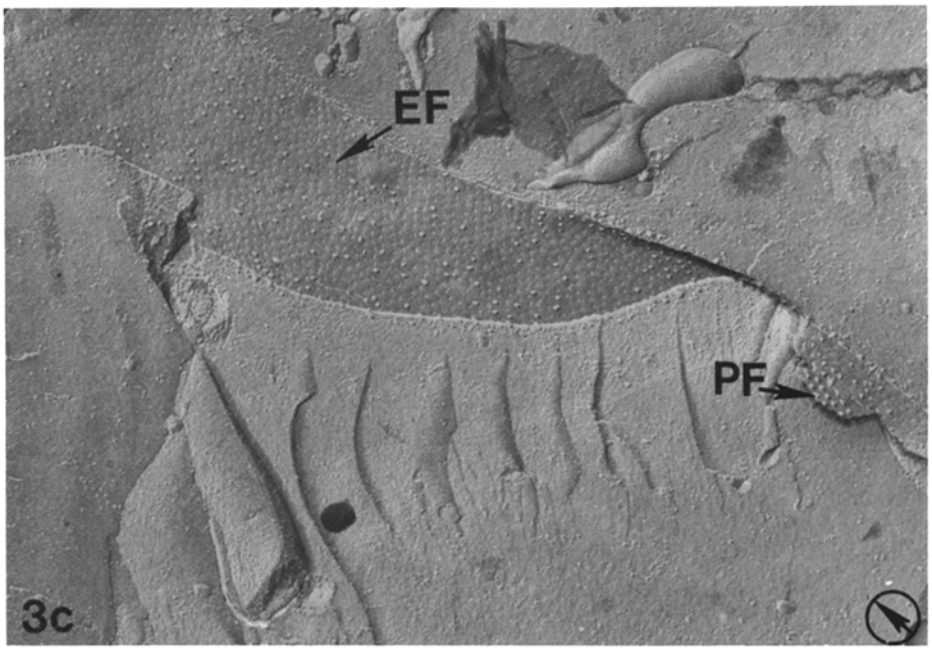

FIGURE 3

Table I shows data from 16 freeze-fractured septa. The total area of the septa is given as well as the average particle density (292 particles/μm^2). Each particle averages 13.5 nm in diameter and from this the total surface area of nexus was determined. Both Matter (1973) and Spira (1971), using thin-sectioned material, showed that intercalated disks of mammalian myocardium contained 10–6% nexus, respectively, which is similar to the total nexus surface area of the septum. It has been proposed that the nexal particles contain a channel (2.0 nm in diameter; Weingart, 1974). Each conducting channel is presumably surrounded by insulation material. Using the total surface area of the channels to calculate permeability gives high values because the total surface of channels cannot account for frictional forces and charges that may be present in each channel which would tend to increase the resistivity of each channel. In addition, access to the total surface area would be much easier than to any one 1.5- to 2.0-nm channel of many million present. Table I also gives values for total nexus surface area and total "channel" area. These areas were computed using the mean particle density of 292 particles/μm^2.

The loss of total area under the curves from one time to another may be considered the result of the loss of dye which diffuses through the plasma membrane or inactivation of dye molecules due to previous light exposure (quenching) or a combination of both events. If it is assumed that for every photographic exposure 1% of total area is lost as a result of quenching and that any other loss is owing to efflux of the dyes across the plasma membrane, then a plasma membrane permeability can be computed for each dye. The computation is the same as that for septal membrane permeability using the cell surface area minus the septal membrane nexal surface area. Inasmuch as the dyes are

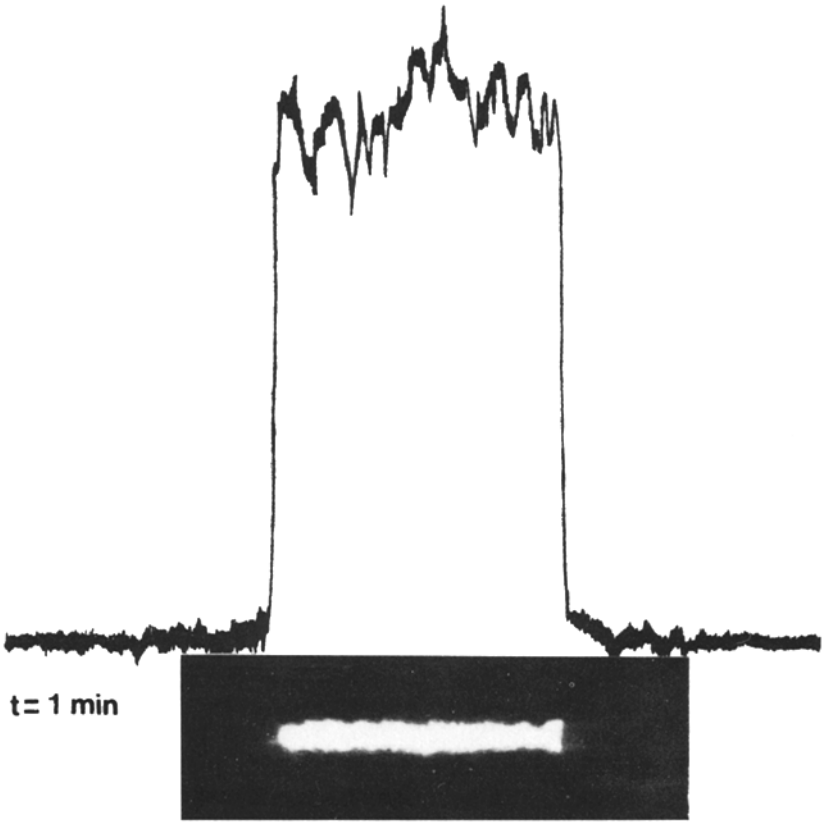

FIGURE 4. A dye injection is shown where the photographs were taken 1 and 15 min after dye injection termination. Densitometric tracings of the negative used to make the prints are also shown. Note the shift in the curve indicating movement of dye through the septa.

negatively charged and the dyes are moving through the plasma membrane (V_m = −80 mV), Eq. 3 was used to compute plasma membrane permeability. The ratio of nexal membrane permeability to plasma membrane permeability is given in Table III. For both aminofluorescein and tetraiodofluorescein <1% of the area was lost, making accurate calculations of plasma membrane permeability impossible. Tetraiodofluorescein was difficult to iontophorese into the axon in concentrations large enough to record fluorescence. In those cases where fluorescence could be observed, no dye could be observed traversing the septa.

Aminofluorescein had a septal membrane permeability of 5.1×10^{-7} cm/s, taking into account the binding. If no binding occurred, the permeability would be 2.5×10^{-7} cm/s. During and after aminofluorescein iontophoresis, the action potential and resting potential showed no significant change, but after 2 h some depolarization was observed.

A summary of septal membrane permeability and flux to the various dyes across the septal membranes is given in Table III. Note that both permeability and flux decrease with increasing molecular weight. Permeability of septal

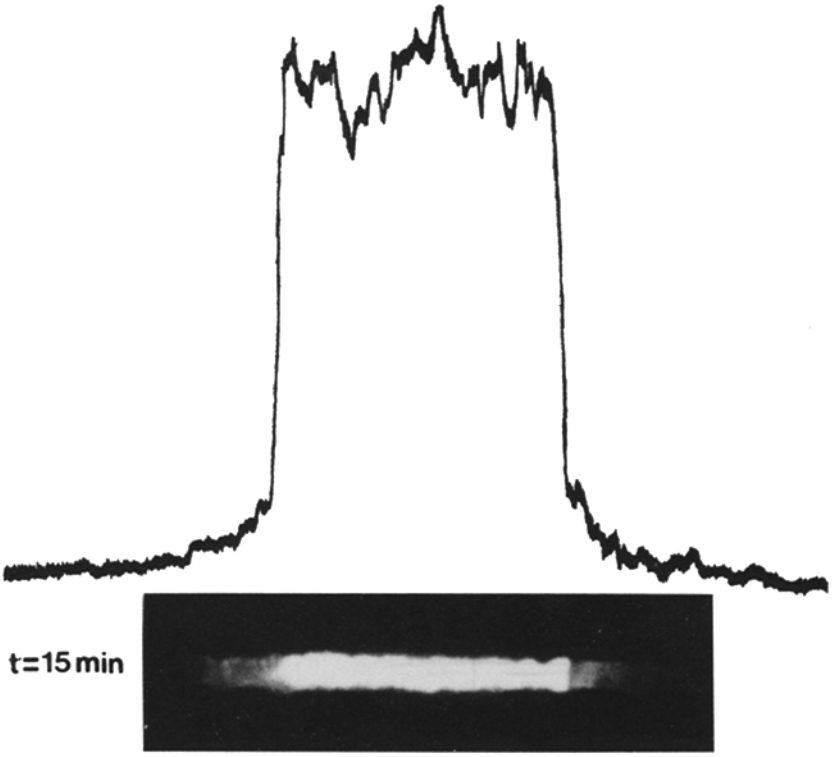

FIGURE 4

TABLE III

NEXAL AND PLASMA MEMBRANE PERMEABILITY

Dye	Nexal membrane permeability (total nexus surface area)		Nexal membrane flux		Mean plasma membrane permeability		(P_n/P_m)*
	cm/s	*SD*	*mol/cm²·s*	*SD*	*cm/s*	*SD*	
Fluorescein	5.4×10^{-5} (n=8)	1.2×10^{-5}	2.2×10^{-11}	1.6×10^{-11}	1.2×10^{-8}	5.0×10^{-9}	4,500
Dichlorofluorescein	3.8×10^{-5} (n=10)	1.6×10^{-5}	1.6×10^{-11}	5.0×10^{-12}	1.0×10^{-8}	5.6×10^{-9}	3,800
Dibromofluorescein	3.0×10^{-5} (n=6)	1.4×10^{-5}	1.3×10^{-11}	7.3×10^{-12}	1.1×10^{-8}	4.5×10^{-9}	2,727
Diiodofluorescein	1.6×10^{-5} (n=6)	8.0×10^{-6}	1.3×10^{-12}	5.4×10^{-13}	7.1×10^{-9}	4.0×10^{-9}	2,253
Tetrabromofluorescein	4.0×10^{-6} (n=6)	2.0×10^{-6}	7.0×10^{-13}	5.3×10^{-13}	2.0×10^{-8}	8.0×10^{-9}	200
Aminofluorescein	5.1×10^{-7} (n=4)	1.6×10^{-7}	1.6×10^{-13}	4×10^{-14}	$>1.0\times10^{-8}$		410

* Nexal membrane permeability/plasma membrane permeability.

membranes to the six probes is graphed against molecular weight in Fig. 5. The correlation coefficient for the line drawn through the points is −0.95.

Examples of microdensitometric scans of a fluorescein injection are shown in Fig. 6. The time intervals were 4, 50, and 90 min. From tracings like those of Fig. 6, permeability at varying time intervals was calculated and permeability remained constant for any of the dyes used. The densitometric tracings indicate that dye moved across the septa and diffused through the axoplasm. It can be seen from the tracings that the system moved toward equilibrium. The nexal membrane permeability calculated from Fig. 6 for the 50-min time interval was 6.0×10^{-5} cm/s and 5.7×10^{-5} cm/s for the 90-min interval. In Fig. 5 the total

area decreased by 5.5% with the 50-min interval and 9% with the 90-min interval. Taking quenching into account (1% loss with each exposure), the total dye movement across the plasma membrane was 4.5% for 50 min and 7% for 90 min. There should be a lesser loss of dye across the plasma membrane between the 50- and 90 min interval because the dye concentration had decreased in the injected cell. The calculated plasma membrane permeability for the 50-min interval was 8.9×10^{-9} cm/s and for the 90-min interval it was 8.1×10^{-9} cm/s with a calculated initial dye concentration of 0.4 mM fluorescein and a cell

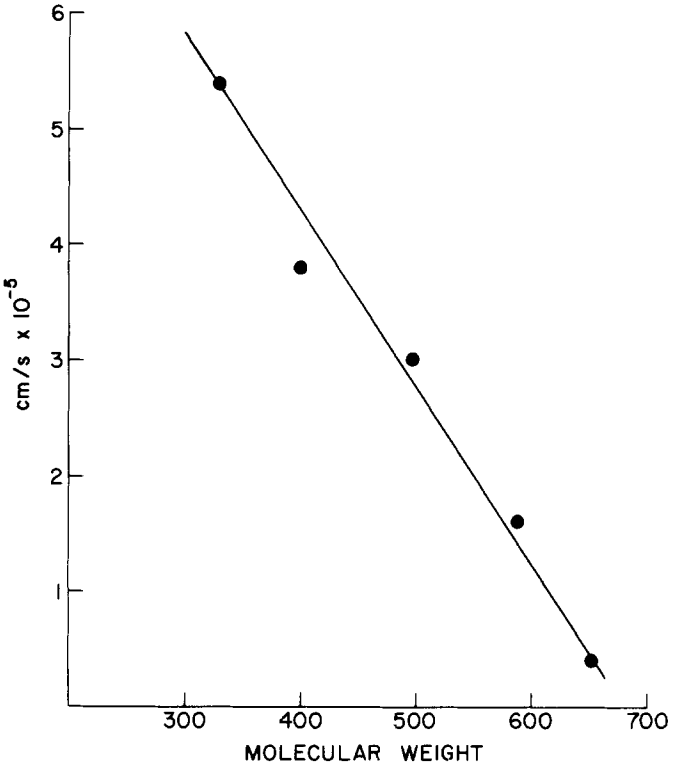

FIGURE 5. Molecular weight of the probes used vs. permeability was plotted. Fluorescein has a mol wt of 333, dichlorofluorescein is 401, dibromofluorescein is 490, diiodofluorescein is 588, and tetrabromofluorescein is 652.

volume of 3.0 nl. The profiles of the injected cell showed considerable variation in density. The fact that the axon at normal body length is folded in an accordion-like fashion may explain an otherwise unexplainable variation in the densitometric scan.

Correlation of Data with Passive Diffusion

A diffusion model system such as two cylinders filled with solutions of similar composition and an interfacing resistance is equivalent to adjacent axoplasms interfaced by the nexal membrane of the septum. Diffusion in this system can be described by:

$$D\frac{\partial^2 C}{\partial x^2} = \frac{\partial C}{\partial t}, \tag{4}$$

where D is the diffusion coefficient (cm^2/s) and C is the concentration. The interface or septum is located at $x = 0$.

It is assumed that the concentration of the diffusing solute in the region $x > 0$ is uniform (C_0) at $t = 0$ and for $x < 0$ the concentration is zero for $t = 0$. C_1 will denote the concentration for $x > 0$. C_2 will denote the concentration for $x < 0$.

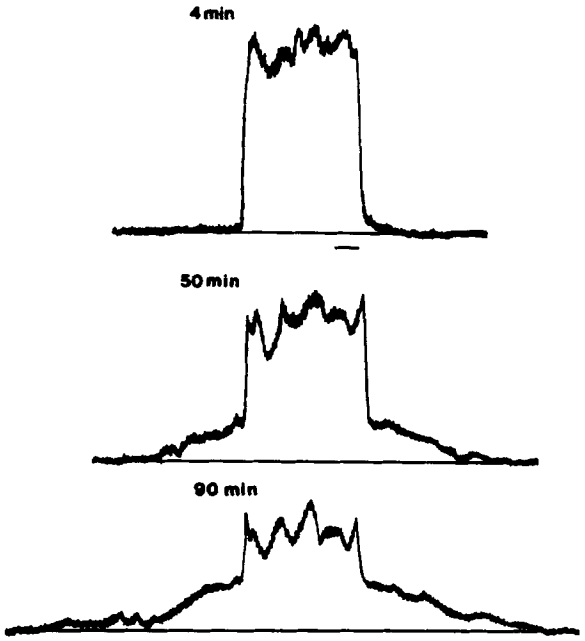

FIGURE 6. Fluorescein was iontophoresed into an axon for 15 min. Photographs were taken 4, 50, and 90 min after the iontophoretic period ended. Densitometric tracings of the three negatives were made. The line drawn at the base of each trace served as a base line for area and amplitude calculations. Note that the tracings indicate dye movement into adjacent cells. The decrease in density (therefore concentration) is roughly exponential with distance along the axon. The horizontal bar under the first tracing represents a distance of 200 μm. Permeabilities calculated for the various time intervals were the same.

The two boundary conditions are (*a*) $D_1\frac{\partial C_1}{\partial x} = D_2\frac{\partial C_2}{\partial x}$ at $x = 0$, and (*b*) $D_1\frac{\partial C_1}{\partial x} = P_n(C_2 - C_1) = 0$ at $x = 0$ where P_n = permeability (cm/s) across the interphase. D_1 is the diffusion coefficient for $x > 0$ and D_2 is the diffusion coefficient for $x > 0$ and $D_2 = D_1$. The nexal membrane permeability of the interphase equals P_n. Integration leads to solutions for C_1 and C_2 as a function of distance and time which are given by Crank (1956, p. 40). The cylinders with an interphase at $x = 0$ are assumed to go on to plus and minus infinity whereas the distance from septum to septum is usually 1–2 mm (Brink and Barr, 1977). Therefore short time intervals after injection were used to allow comparison of experimental

results with the diffusion model system because short time intervals would allow the best possible approximation of the boundary conditions.

Two examples of comparisons between experimental and theoretical results are given in Fig. 7. Fig. 7A shows (left-hand side) a densitometric trace from negatives made of a dichlorofluorescein injection of the axon. The photographs were made 30 s and 3 min after termination of injection period. The permeability computed from the densitometric tracings was 2.1×10^{-5} cm/s. Fig. 7A (right-hand side) also contains curves of C_1 and C_2 gotten from the Crank formalization made at $t = 30$ s and 3 min where the interphase permeability was 2×10^{-5} cm/s and the diffusion coefficient was 5×10^{-7} cm^2/s. At $t = 0$, $C_1 = 1$ and $C_2 = 0$. Fig. 7B shows densitometric traces of negatives taken 1 and 16 min after termination of the iontophoresis of dibromofluorescein. The permeability calculated from these tracings was 1×10^{-5} cm/s. Tracings of C_1 and C_2 are shown at 1 and 15 min where the interphase permeability was 7×10^{-6} and the diffusion coefficient was 9×10^{-8}. Once again at $t = 0$, $C_1 = 1$ and $C_2 = 0$. These examples are used to show a correlation between the densitometric data and the diffusion model. From the comparison it is apparent that the dyes are moving through the septa via passive diffusion processes. One important difference is the behavior of the injected cell region of the densitometric tracing and that of the C_1 region. This disparity has as yet no full explanation.

In all cases the permeabilities calculated from densitometric tracings when used in the Crank (1956) equations gave tracings of C_2 that were in good agreement with the densitometric tracings. The diffusion coefficients for fluorescein was 1×10^{-6} cm^2/s, 5×10^{-8} cm^2/s for diiodofluorescein, and 1×10^{-8} cm^2/s for tetrabromofluorescein. In each case, short time intervals of $\leqq 16$ min were used. In each instance only one densitometric trace per dye was analyzed with respect to the Crank equations. Fig. 8 is a comparison of nexal membrane permeability of various probes (Weidmann, 1966; Weingart, 1974; Pollack, 1976), including those of this study. Permeability is plotted against molecular weight of the probes. In all these cases the total nexus surface area is used in computation of flux data from which permeability is computed.

DISCUSSION

The molecular weight of the fluorescent probes used here varied from 333 to 652, and the nexal membrane permeability varied from 5.4×10^{-5} to 4.0×10^{-6} cm/s using the nexus surface area as the conduction proportion of the septal membrane.

Calculation of the potassium permeability can be made from the resistance data (Brink and Barr, 1977) and use of the equation:

$$G_K = K_1 \times P_K \times (F^2/RT) \quad \text{(Weidmann, 1966)}, \tag{5}$$

where G_K = conductance of the disk for potassium ions, P_K = permeability of disk to potassium, F, R, and T have their usual significance,

K_1 = potassium concentration in the myoplasm. If the disk conductance and permeability to potassium is assumed to be nexal membrane conductance and permeability, then Eq. 5 can be rearranged so that

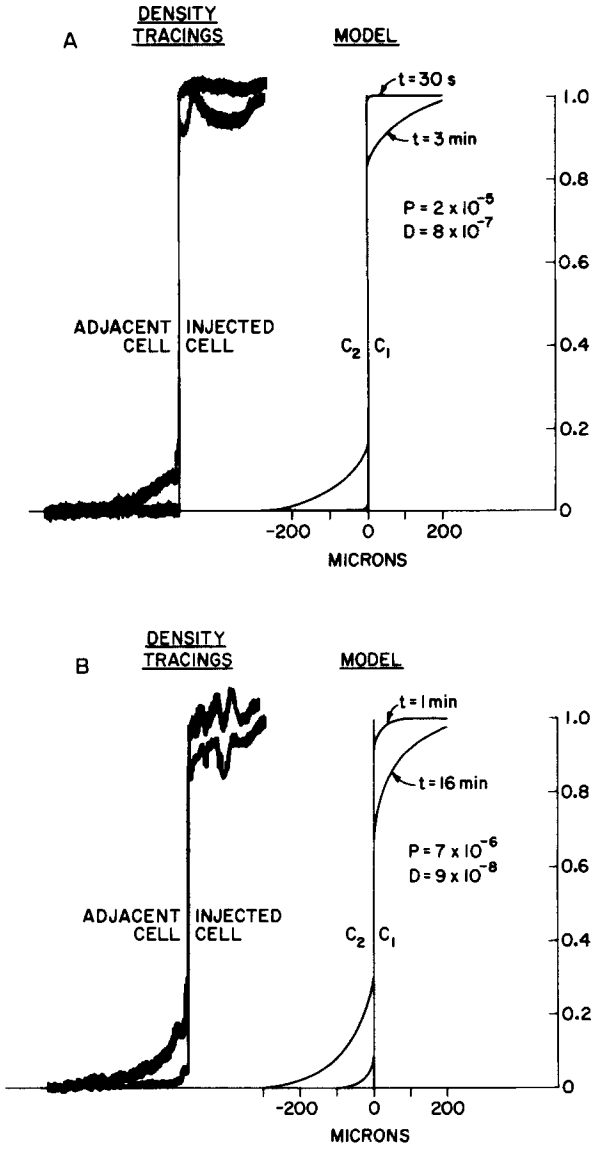

FIGURE 7. (A) Comparison of densitometric tracing made from negatives of a dichlorofluorescein injection and the Crank equations (1956). Photographs were made 30 s and 3 min after termination of dye injection. D = diffusion coefficient and P = permeability. The permeability computed from the densitometric tracings was 2.1×10^{-5} cm/s. Densitometric data are displayed on the left side of the figure, curves from the Crank formalism are shown on the right. On the right, values of x from 0 to negative values of x represent the adjacent cell whereas positive values of x represent the injected region. (B) A similar comparison to A only the dye used was dibromofluorescein. The permeability computed from densitometric tracings was 1×10^{-5} cm/s (left side).

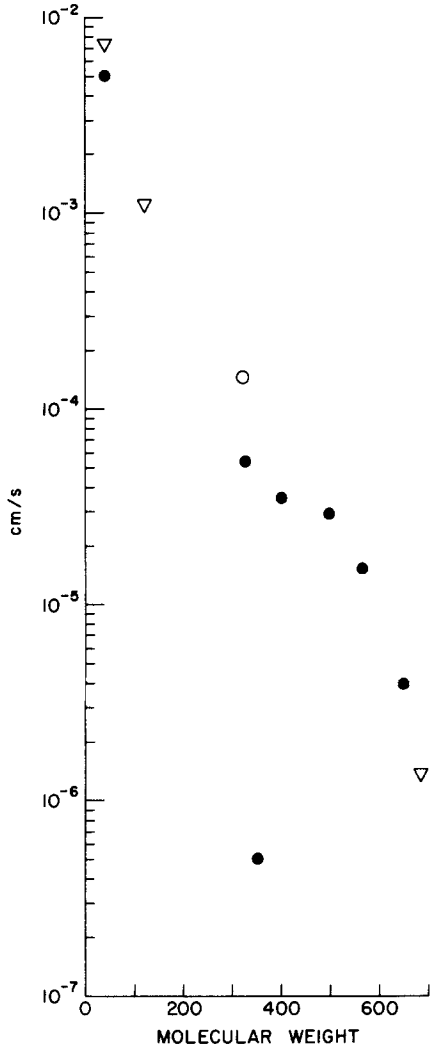

FIGURE 8. Semi-log plot of permeability vs. molecular weight. Triangles are values taken from Weingart (1974). The open circle is a value for fluorescein taken from Pollack (1976). Filled circles are data present in Fig. 5. The data for aminofluorescein are also shown. Molecules summarized by Weingart (1974) were K^+, tetraethylammonium (TEA), and Procion Yellow.

$$P_K = \frac{G_K}{K_1 \times (F^2/RT)}, \tag{6}$$

where P_K is the nexal membrane permeability to potassium.

Brink and Barr (1974, 1977) calculated a nexal membrane resistance of 6 ohm cm^2 in the septa of the median giant axon of earthworm. Using the surface area data presented here, the resistance of the nexal membrane drops to 0.3 ohm cm^2 for the nexal membranes of the septa. If it is assumed that the internal

potassium ion concentration is 150×10^{-6} mol/cm^3, then the P_K for the septal nexus can be computed from Eq. 6 to be 5.0×10^{-3} cm/s.

McNutt and Weinstein (1973) and Matter (1973) from morphological studies estimated the nexal membrane pore to be between 1.0 and 1.5 nm in diameter. Radioactive K^+, TEA, and Procion Yellow were able to traverse a nexal membrane, indicating that the pore was approximately 1.0 nm. In the developing squid the dye Chicago Blue (1,000 mol wt) could traverse nexal membranes (Potter et al., 1966). The molecular dimensions of Chicago Blue are not known. Models of fluorescein, dichlorofluorescein, dibromofluorescein, diiodofluorescein, tetrabromofluorescein, and aminofluorescein were made using conventional bond angles and lengths. The probes vary in their widest dimension from 0.9 to 1.3 nm. Inasmuch as all the probes except aminofluorescein are negatively charged at physiological pH, they are assumed not to be hydrated. The largest diameter is 1.3 nm, therefore the pore must be at least 1.3 nm in diameter to accommodate such molecules (tetrabromofluorescein). The largest dimension of tetraiodofluorescein is 1.4 nm.

The comparison of the densitometric tracings with solutions of a diffusion model given by Crank (1956) are good with respect to the adjacent cell region and the solution of C_2. The permeabilities used for the model are the same or similar in magnitude to those computed from the densitometric tracings. However, there is not as good a correspondence between densitometric tracings of injected cell regions and C_1 with varied time. Possible explanations for this may be some change of the diffusion coefficient in the injected cell region due to high dye concentration, or possibly some form of axoplasmic flow not seen with low concentrations of dye in adjacent segments. There may be many other explanations for this presently unexplainable derivation from theory.

Estimates of cellular dye concentration were undertaken to determine whether the amount of dye injected was changing the osmotic conditions of the cell significantly and to allow an estimate of the concentration gradient across the nexus. Figs. 1 and 2 were used as standard curves to estimate dye concentration in the cytoplasm. There was no case where the amplitude of a densitometric trace exceeds that of Fig. 1. Variations in Fig. 1 may be the result of wall thickness differences.

If the permeabilities are calculated using just the "channel" surface area, then the permeabilities are raised by a factor of approximately 50. Therefore, the fluorescein permeability would be 2.7×10^{-3} cm/s. Use of values this high in the Crank (1956) model bring the model to equilibrium within 10–20 min and the diffusion across the interphase greatly exceeds that of the densitometric tracings. Assuming that the permeability of fluorescein to the septa which best fits the Crank equations is correct (5.4×10^{-5} cm/s) and that each particle has a 1.5- to 2.0-nm channel, then the channels have a factor of 50 greater resistance to diffusion than axoplasm.

Another point is the use of short time intervals for analysis of computed data and the Crank equations. With short time intervals, used just after injection termination, good agreement for permeability values was possible. If longer intervals were used (30–50 min), the permeability value used in the Crank model

was always less than the computed value by a factor of 2–5. This error is most likely due to the fact that at longer time intervals the experimental computed values are gotten under conditions where the boundary conditions are not met for the model. Fig. 5 shows an apparent linear relationship for permeability vs. molecular weight, and this may be due to the fact that surface charge density of the molecules is different. Plotting the points on a logarithmic plot shows that they all fall in the range of other probes used on nexal membranes (Fig. 8).

The permeability of aminofluorescein to nexal membranes is much lower than the permeability of any of the anion dyes. The reasons for this may be that aminofluorescein binds to nexal membranes as it does to cytoplasmic proteins or that the net charge of aminofluorescein is different from those of fluorescein, dichlorofluorescein, dibromofluorescein, diiodofluorescein, and tetrabromofluorescein. Fluorescein and the fluorescein halogen derivatives would have a net negative charge at physiological pH whereas aminofluorescein would have a net positive charge or be neutral.

The nexal membrane permeability in the septum of the median giant axon of earthworm ranges from 5.4×10^{-5}–4.0×10^{-6} cm/s for mol wt of 333–652. The three-dimensional structure of the individual dyes will determine their ability to diffuse across the nexus, but the data given here would suggest that molecules in the range of 1,000 mol wt represent the upper limit for molecules to diffuse across a nexal membrane.

The authors would like to thank Dr. L. Barr for helpful discussions and Ms. E. Petite for technical assistance.

This work was supported by grant GM-05231 from the National Institutes of Health.

Received for publication 2 March 1978.

REFERENCES

BARR, L., W. BERGER, and M. M. DEWEY. 1968. Electrical transmission at the nexus between smooth muscle cells. *J. Gen. Physiol.* **51**:346–368.

BARR, L., M. M. DEWEY, and W. BERGER. 1965. Propagation of action potentials and structure of the nexus in cardiac muscle. *J. Gen. Physiol.* **48**:797–823.

BENNETT, M. V. L., G. D. PAPPAS, E. ALJURE, and Y. NAKAJIMA. 1967. Physiology and ultrastructure of electrotonic junctions. II. Spinal and medullary electromotor nuclei in moryrid fish. *J. Neurophysiol.* **30**:180–208.

BERLMAN, I. 1971. Handbook of Fluorescence Spectra of Aromatic Molecules. Academic Press, Inc., New York. 2nd ed.

BRANTON, D., S. BULLIVANT, N. B. GILULA, M. J. KARNOVSKY, H. MOORE, K. MÜHLETHALER, D. H. NORTHCOTE, L. PACKER, B. SATIR, V. SPETH, L. A. STAEHLIN, R. L. STEERE, and R. S. WEINSTEIN. 1975. Freeze-etching nomenclature. *Science (Wash. D. C.)*. **190**:54–56.

BRINK, P., and L. BARR. 1974. The specific resistance of a nexus in the earthworm. *Fed. Proc.* **33/3**:319.

BRINK, P., and L. BARR. 1977. The resistance of the septum of the median giant axon of the earthworm. *J. Gen. Physiol.* **69**:517–536.

BRINK, P., and M. M. DEWEY. 1976. Permeability of the septum in the median giant axon earthworm to various dyes. General Physiologists Meetings, Woods Hole, Mass., September 1976.

BULLOCK, T., and G. H. HORRIDGE. 1965. Structure and Function in the Nervous Systems of Invertebrates. Vol. I. W. H. Freeman & Company, San Francisco. 104, 689–707.

COX, R. P., M. R. KRAUSS, M. E. BALIS, and J. DANCIS. 1974. Metabolic cooperation in cell culture. *In* Cell Communication. R. P. Cox, editor. John Wiley & Sons Inc., New York. 67–96.

CRANK, J. 1956. The Mathematics of Diffusion. Oxford University Press, London. 1st edition.

DEWEY, M. M., and L. BARR. 1964. A study of the structure and distribution of the nexus. *J. Cell Biol.* **23**:553–585.

FARQUHAR, M., and G. PALADE. 1963. Junctional complexes in various epithelia. *J. Cell Biol.* **17**:375–412.

FURSHPAN, E. J., and D. D. POTTER. 1959. Transmission at giant synapses of the crayfish. *J. Physiol. (Lond.).* **145**:289–325.

GILULA, N. 1974. Junctions between cells. *In* Cell Communication. R. P. Cox, editor. John Wiley & Sons Inc., New York. 1–29.

GILULA, N. B., O. R. REEVES, and A. STEINBACH. 1972. Metabolic coupling, ionic coupling and cell contracts. *Nature (Lond.).* **235**:262–264.

GOLDMAN, D. E. 1943. Potential, impedance, and rectification in membranes. *J. Gen. Physiol.* **27**:37–59

GUNTHER, J. 1971. Der cytologische Aufbau der dorsalen Riesenfaser von *Lumbricus terrestris*. *L. Z. Wiss. Mikrosk. Mikrosk. Tech.* **183**:51–70.

GUNTHER, J. 1975. Neuronal synctia in the giant fibers of earthworm. *J. Neurocytol.* **4**:55–62.

HAMA, K. 1959. Some observations on the fine structure of the giant nerve fibers of the earthworm *Eisenia* foetida. *J. Biophys. Biochem. Cytol.* **6**:61–66.

HODGKIN, A. L., and B. KATZ. 1949. The effect of sodium ions on the electrical activity of the giant axon of the squid. *J. Physiol. (Lond.).* **108**:37–77.

IMANAGA, I. 1974. Cell to cell diffusion of Procion Yellow in sheep and calf Purkinje fiber. *J. Membr. Biol.* **16**:381–388.

KAO, C. Y., and H. GRUNDFEST. 1957. Postsynaptic electrogenesis in septate giant axons. I. Earthworm median giant axon. *J. Neurophysiol.* **20**:553–573.

KATZ, B. 1966. Nerve, Muscle, and Synapse. McGraw-Hill Book Company, New York. 60–62.

LOEWENSTEIN, W. R. 1975. Permeable junctions. *Cold Spring Harbor Symp. Quant. Biol.* **XL**:49–64.

MARTIN, A. R., and G. PILAR. 1963. Dual mode of synaptic transmission in avian ciliary ganglion. *J. Physiol. (Lond.).* **168**:443–463.

MATTER, A. 1973. A morphometric study on the nexus of rat cardiac muscle. *J. Cell Biol.* **56**:690–696.

MCNUTT, N., and R. WEINSTEIN. 1973. Membrane ultrastructure of mammalian intercellular junctions. *Prog. Biophys. Mol. Biol.* **26**:45–101.

PAPPAS, G. D., Y. ASADA, and M. V. L. BENNETT. 1971. Morphological correlates of increased coupling resistance at an electrotonic synapse. *J. Cell Biol.* **49**:173–188.

PAPPAS, G. D., and M. V. L. BENNETT. 1966. Electrical transmission between neurons. *Ann. N. Y. Acad. Sci.* **137**:495–528.

POLLACK, G. H. 1976. Intercellular coupling in the atrioventricular node and other tissues of rabbit heart. *J. Physiol. (Lond.).* **255**:275–298.

POTTER, D. D., E. J. FURSHPAN, and E. S. LENNOX. 1966. Connections between cells of developing squid. *Proc. Natl. Acad. Sci. U.S.A.* **55**:328–336.

PROSSER, C. L., and F. A. BROWN. 1950. Comparative Animal Physiology. W. B. Saunders Company, Philadelphia. 75.

ROBERTSON, J. D. 1963. The occurrence of a subunit pattern in the unit membranes of club endings in Mauthner cells synapses in goldfish brains. *J. Cell Biol.* **19**:201–221.

SPIRA, A. W. 1971. The nexus in the intercalated disc of the canine heart: quantitative data for an estimation of its resistance. *J. Ultrastruct. Res.* **34**:409–425.

STOUGH, H. 1930. Giant nerve fibers of the earthworm. *J. Comp. Neurol.* **50**:217–229.

SUBAK-SHARPE, J. H., R. R. BURKE, and J. D. PITTS. 1969. Metabolic cooperation between biochemically marked cells in tissue culture. *J. Cell Sci.* **4**:353–367.

WEIDMANN, S. 1966. The diffusion of radiopotassium across intercalated discs of mammalian cardiac muscles. *J. Physiol. (Lond.)*. **187**:323–342.

WEINGART, R. 1974. The permeability to tetraethylammonium ions of the surface membrane and the intercalated discs of sheep and calf myocardium. *J. Physiol. (Lond.)*. **240**:741–762.